

Poly(fluorenyl alkylene)-based anion exchange membranes for ¹ high-performance water electrolysis

Yichang Ma ^a, Lingjing Li ^a, Xueqing You ^a, Huiting Lin ^a, Guiqin Yi ^a, Xiangyu Su ^{a,b}, Aimei Zhu ^a, ² Qinglin Liu ^a, Qiugen Zhang ^{a,b,*}

^a State Key Laboratory of Physical Chemistry of Solid Surfaces, College of Chemistry and Chemical Engineering, Xiamen University, Xiamen 361005, China ³

^b Innovation Laboratory for Sciences and Technologies of Energy Materials of Fujian Province (IKKEM), Xiamen 361102, China

ARTICLE INFO ⁴

Keywords:
Anion exchange membrane ⁶
Water electrolysis
Poly(aryl alkylene)
Hydrogen production

ABSTRACT ⁵

Durable and high-performance anion exchange membranes (AEMs) are a pivotal issue for the industrial application of AEM water electrolysis (AEMWE). In this study, a series of poly(fluorenyl alkylene) copolymers with different contents of biphenyls and *p*-terphenyls are synthesized for the high-performance AEMWE. The resulting AEM with an appropriate content of *p*-terphenyl well facilitates the microphase separation to get a well-defined microstructure that effectively improves the ionic conductivity and reduces the swelling ratio. The AEM with 20% *p*-terphenyl possesses an OH⁻ conductivity of 155.7 mS cm⁻¹, a water uptake of 128.7%, and a swelling ratio of 33.8% at 80 °C. Moreover, it also shows durable alkaline stability and retains 83.5% of cationic groups after immersing in 5 M NaOH at 80 °C for 1440 h. The assembled AEMWE cell achieves an excellent current density of 4.9 A cm⁻² at 2 V in 1 M KOH (80 °C) and 2200 h of long-term constant current (1 A cm⁻²) operation with a low voltage rising rate of 77 µV h⁻¹. After this long-term operation, only 13.7% of cationic groups are degraded in the AEM, showing excellent *in-situ* durability. Therefore, the developed AEMs should have great potential for applications in the AEMWE. ⁷

1. Introduction ⁸

Hydrogen is an ideal energy carrier for decarbonization and the storage of renewable electricity [1,2]. Water electrolysis driven by electricity from renewable energy sources to produce high-purity hydrogen without carbon emissions is deemed a sustainable method for realizing energy conversion and storage [3–5]. The AEMWE presents distinguished advantages that combine the merits of mature alkaline water electrolysis (AWE) and burgeoning proton exchange membrane water electrolysis (PEMWE) [6,7]. The zero-gap-assembly AEMWE cell with solid polymer electrolyte AEM allows for operations at high currents and generates pressurized and high-purity hydrogen. Meanwhile, the alkaline work environment provides the possibility to use platinum-group-metal-free (PGM-free) catalysts and inexpensive metal hardware [8–10]. However, the AEM and ionomers, as the core components of AEMWE with unsatisfied anion exchange polyelectrolytes (AEPs), still do not guarantee high current density and longevity. Despite the fact that researchers have developed several commercial AEMs and anion

exchange ionomers (AEIs), such as Fumasep® FAA3, PiperION, Aemion™, Sustainion®, and Orion TM1, etc [11–13]. However, higher-performance AEMs are strongly required for the practical application of AEMWE. ⁹

High ion conductivity, robust mechanical properties, and durable chemical stability are essential for ideal AEM and ionomers to meet the harsh work environment due to the strong nucleophilic and basic character of the hydroxide [14,15]. In the past decade, ether-free AEPs, which avoid the issue of aryl ether cleavage reactions in ether-linked polymer backbone, have gradually risen to the forefront of research [16]. Among numerous ether-free AEPs, poly(biphenyl alkylene)s synthesized via Friedel-Crafts alkylation polymerization show many merits, including the simple synthetic process, excellent alkaline stability, and robust mechanical properties owing to the well-defined microphase separation structure caused by the long alkyl side chain structure and small quaternary ammonium ion group tethered to the alkyl spacer [17–20]. For instance, the poly(biphenyl alkylene) has no obvious degradation after soaking in 1 M NaOH at 80 °C for 720 h [21]. In

* Corresponding author at: State Key Laboratory of Physical Chemistry of Solid Surfaces, College of Chemistry and Chemical Engineering, Xiamen University, Xiamen 361005, China.

E-mail address: qgzhang@xmu.edu.cn (Q. Zhang).

addition, introducing a rigid, twisted structure into the main chain is considered an effective way to promote microphase separation and improve conductivity. For instance, the poly(terphenylene) with a meta-terphenyl structure can effectively promote the ion conductivity to 112 mS cm^{-1} at 80°C , higher than the p-terphenyl base poly(terphenylene) (81 mS cm^{-1}) [22].

On the other hand, the interaction between the ionomer and catalyst has a nonnegligible impact on AEMWE performance. Some research on AEM fuel cells (AEMFC) has proved that polyaromatic ionomers with non-rotatable phenyl-phenyl rings have smaller adsorption energies on catalysts, significantly improving AEMFC performance [19,23,24]. In the field of AEMWE, the alkylammonium poly(carbazole)-based AEP QPC-TMA reached a state-of-the-art AEMWE performance of 3.5 A cm^{-2} at 1.9 V [18]. The poly(fluorenyl-co-aryl piperidinium) (PFAP) presented impressive AEMWE current density of 7.68 A cm^{-2} at 2.0 V in 1 M KOH [4]. From these, it is seen that the non-rotatable aromatic structure is a good choice to construct a microphase separation structure and decrease interaction between the ionomer and catalyst.

In this study, a series of ether-free quaternized poly(fluorenyl alkylene) (PFA) AEPs with outstanding AEMWE performance were developed by combining the non-rotatable fluorenyl and flexible alkyl side chains, as shown in Fig. 1a. Biphenyl and p-triphenyl were introduced into PFA to construct poly(fluorenyl-co-biphenyl alkylene) (PFBA) and poly(fluorenyl-co-p-terphenyl alkylene) (PFTA) polymer structures. The microstructures of as-synthesized AEMs were characterized in detail. Furthermore, the water uptake (WU), swelling ratio (SR), ion conductivity (σ), and mechanical properties were investigated to elucidate the relationship between performance and polymer backbone structure. Finally, membrane-electrode assemblies (MEAs) parameters, such as the preparation method of MEAs, ionomer contents, catalyst loading, *et al.*, were optimized to achieve the high performance of AEMWE.

2. Experimental 4

2.1. Materials 5

Biphenyl (99.5%), trifluoromethanesulfonic acid (TFSA, 99%), trifluoroacetic acid (TFA, 99%) and chloroform-d ($\text{CDCl}_3\text{-d}$, 99.8 atom%D) were purchased from *J&K Chemical Ltd*. Trimethylamine (TMA) solution (30 wt% in H_2O) and *p*-terphenyl (99%) were obtained from *Aladdin Biochemical Technology Co., Ltd*. Dimethyl sulfoxide-d₆ (DMSO-d₆, 99.8 atom%D) was obtained from *Beijing InnoChem Science & Technology Co., Ltd*. 7-bromo-1,1,1-trifluoroheptan-2-one (BtFHO) was supported by *Xiamen Kah Membrane Technology Ltd*. Ultra-pure water is manufactured by Milli-Q ($>18.2 \text{ M}\Omega \text{ cm}^{-1}$). Other chemicals were purchased from *Sinopharm Chemical Reagent Co., Ltd*.

2.2. Synthesis of poly(fluorenyl alkylene) copolymers 7

Bromoalkyl-tethered poly(fluorenyl alkylene) (PFBr): 1.76 g (9.06 mmol) of 9,9-dimethylfluorene and 2.53 g (10.22 mmol) of BtFHO were dissolved in 6 ml of dichloromethane (DCM) in a 100 ml round-bottom flask. After dissolving evenly, 5 ml of TFSA was added and reacted at ambient temperature for 3 h. After the reaction solution became highly viscous, it was precipitated into methanol, filtered to obtain massive structure polymer. Then, redissolved in DCM and precipitated in methanol two times repeatedly. After that, the obtained fibrous form polymer was collected and filtered, and dried at 80°C for 24 h to obtain PFBr.

The bromoalkyl-tethered poly(fluorenyl-co-biphenyl alkylene)s (PFBr-x, the x represents the percentage proportion of biphenyl, here x = 75): 2.77 g (17.98 mmol) of biphenyl, 1.17 g (6.01 mmol) of 9,9-dimethylfluorene, 6.51 g (26.36 mmol) of BtFHO, and 16 ml of DCM were added in a 100 ml round-bottom flask, and stirring ensures uniform dissolution. After that, 16 ml TFSA added slowly. The reactant solution

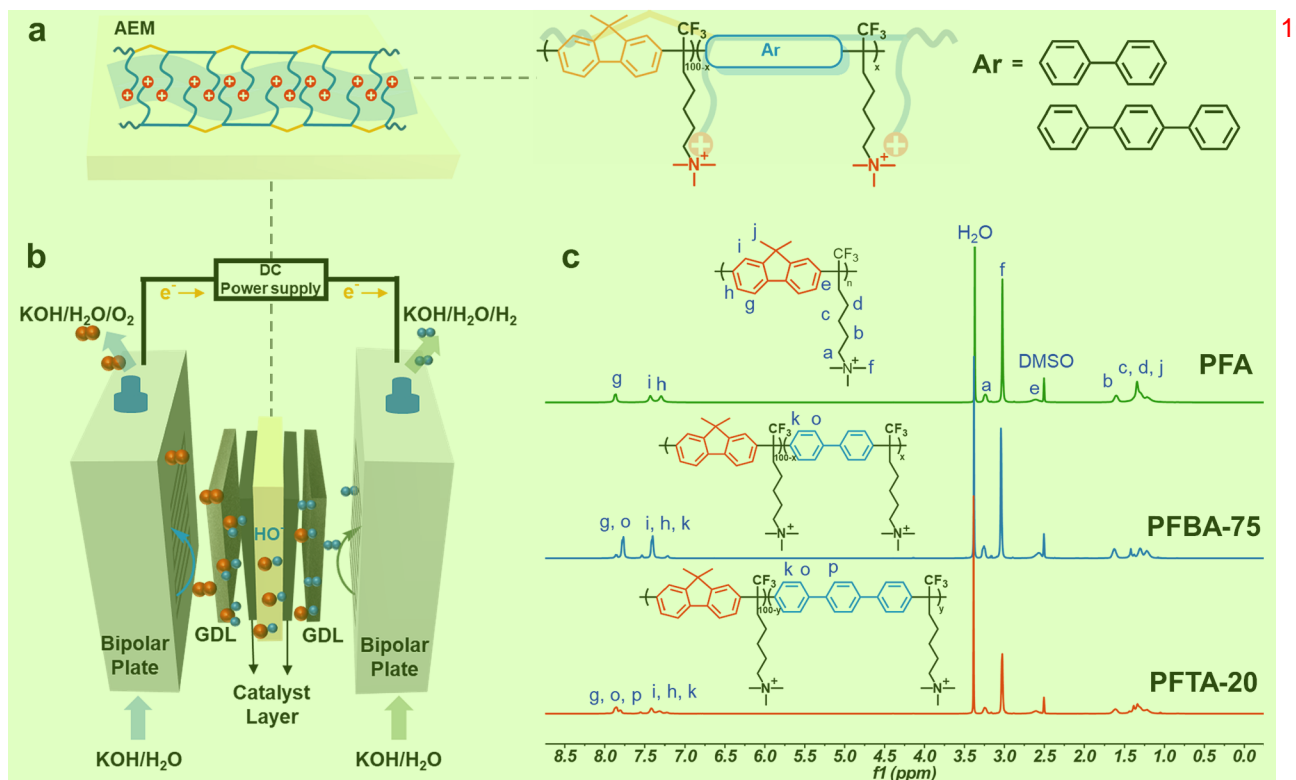


Fig. 1. (a) Schematic illustration of the construction of internal ion channels in PFA-based AEMs and the chemical structures of PFA-based AEMs. (b) Schematic of AEMWE equipment with PFA-based AEMs. (c) ¹H NMR spectra of PFA, PFBA-75 (75 represents the percentage proportion of biphenyl) and PFTA-20 (20 represents the percentage proportion of p-triphenyl).

was reacted at room temperature for 5 h, and the treating processes were the same as for PFBr. While, with the increase in fluorenyl content in PFBA, PFBA-50 is too brittle to form a membrane.

Bromoalkyl-tethered poly(fluorenyl-co-*p*-terphenyl alkylene)s (PFTBr-*y*, the *y* represents the percentage proportion of *p*-terphenyl) were synthesized via the same synthesis process of PFBA-75 but replaced biphenyl with *p*-terphenyl. PFTBr-20, PFTBr-50 and PFTBr-75 were synthesized in this study.

Finally, bromoalkyl-tethered copolymers reacted with TMA to obtain PFA, PFBA-*x* (*x* represents the percentage proportion of biphenyl), and PFTA-*y* (*y* represents the percentage proportion of *p*-triphenyl), according to our previous work [25].

2.3. Membrane preparation and ion exchange

The PFA-based AEMs were prepared via the traditional solution casting and ion exchanging process [26]. For instance, 1.8 g of PFA was dissolved in 60 ml of DMSO to form a 3 wt% homogeneous solution, which was filtered by 0.45 µm PTFE filter. The resulting casting solution was poured to clean glass plate and followed by drying at 80 °C for 24 h and another 24 h in a vacuum oven at 80 °C to remove the remaining solvent. A transparent membrane (Br⁻ form) with a thickness of 50 ± 5 µm was obtained. This membrane was soaked in 1 NaOH at room temperature for 24 h to exchange the Br⁻ into OH⁻. Finally, the expected PFA AEM was obtained.

2.4. Characterizations

Chemical structure of as-synthesized copolymers was characterized by ¹H nuclear magnetic resonance (NMR) spectrometer (Bruker Advance III 400 MHz, Switzerland) with CDCl₃-d₁ and DMSO-d₆ as solvent. Morphology of AEMs were observed by scanning electron microscopy (SEM) (Zeiss GeminiSEM 500, Germany). Atomic force microscopy (AFM) (Oxford Instruments Asylum Research Cypher ES, UK) and small angle X-ray scattering (SAXS) (Anton Paar, Austria) were observed the microphase structure of AEMs. The thermal stability was investigated by a thermogravimetric analyzer (SDT-Q600, TA instruments, USA) in N₂ atmosphere from 90 to 800 °C with a heating speed of 10 °C min⁻¹. Furthermore, the mechanical property was measured via universal material testing machine (microtester 5948, Instron, USA) with stretching rate of 1 mm cm⁻¹.

2.5. Measurements of ion exchange capacity (IEC) and ionic conductivity

The back titration technique was used to determine the IEC of as-prepared AEMs. The sample in the OH⁻ form was dried in vacuum oven at 80 °C for 24 h. Subsequently, the sample was immersed into the 40 ml of 0.1 M HCl for 24 h. After soaking, the resulting HCl solution was titrated with 0.1 M NaOH and a small amount of phenolphthalein as an indicator. Then, the IEC was calculated by

$$IEC = \frac{V_{HCl}C_{HCl} - V_{NaOH}C_{NaOH}}{m_{dry}} \quad 10 \quad (1)$$

To investigate the in-plane σ of the AEMs, VersaSTAT 3F electrochemical workstation with four-electrode alternating current (AC) impedance spectroscopy (0.1 Hz to 0.1 MHz) was used. The samples were tested in ultrapure water with nitrogen atmosphere to prevent carbonation. The Ohm impedance (*R*, kΩ) was recorded every 10 °C from 30 to 80 °C. The ion conductivity was calculated by

$$\sigma = \frac{L}{RWT} \quad 12 \quad (2)$$

where *L* is the distance between the two electrodes. *T*, *W* and *R* is the thickness, breadth and ohmic resistance of the sample, respectively.

2.6. Swelling experiments

The swelling behavior of prepared AEMs was measured via the traditional immersing method [27]. All samples in OH⁻ form were immersed in deionized water at designed temperature for 12 h to swell fully. After eliminating the surplus water from the sample surface, the weight (*M_{wet}*) and length (*L_{wet}*) of the swollen samples were measured. The weight (*M_{dry}*) and length (*L_{dry}*) of the dry sample were measured after drying in the vacuum oven at 80 °C for 24 h. Then, the WU and SR were calculated by

$$WU(\%) = \frac{M_{wet} - M_{dry}}{M_{dry}} \times 100\% \quad 16 \quad (3)$$

$$SR(\%) = \frac{L_{wet} - L_{dry}}{L_{dry}} \times 100\% \quad 17 \quad (4)$$

Subsequently, to determine the number of water molecules absorbed by each cationic group, the hydration number (*λ*) can be calculated by the formula (5), and the M_{H₂O} is 18 g mol⁻¹ presents the relative molecular mass of water.

$$\lambda = \frac{WU(\%) \times 1000}{IEC \times M_{H_2O}} \quad 19 \quad (5)$$

2.7. Water electrolysis experiments

In this study, IrO₂ (>85%, Sinero, SYi85) and Pt/C (60%, Johnson Matthey HiSPEC 9100), porous nickel foam, and carbon paper (Toray TGP-H-060) were used as catalysts and gas diffusion layers (GDLs) of the anode and cathode, respectively. All the water electrolysis experiments were carried out on a single AEMWE device (KMem® AE01, Xiamen Kah Membrane Technology Ltd.), as our previous published work used [25]. The catalyst slurry with 20 mg ml⁻¹ catalyst was prepared by dispersing catalyst nanoparticles in a water/IPA mixture (v/v = 1/2). Then, the slurry was manually sprayed on two sides of the AEMs to fabricate the catalyst-coated membrane (CCM) (2 × 2 cm) with an IrO₂ loading of 2 mg cm⁻² and a Pt/C loading of 1 mg cm⁻². Finally, the single AEMWE cell was assembled with CCM, GDLs, PTFE-based gaskets (200 µm) and bipolar plates, as shown in Fig. 1b. Besides, except for pure water and 0.1 M KOH, which were chosen to explore the influence of the electrolyte on the AEMWE performance, other AEMWE tests were carried out in 1 M KOH. The electrolyte circulation flow rate was 3.0 ml min⁻¹.

The influence of ionomer content and type was investigated. The electrochemical impedance spectroscopy (EIS) was recorded by the electrochemical workstation (VersaSTAT 3F) during the single-cell operation at a constant current density of 1 A cm⁻². And the EIS was fitted by the equivalent circuit model (Fig. S13) as reported in previous published work [6,9]. To compare the preparation method of MEA, the catalyst slurry was sprayed on GDL to make catalyst-coated substrate (CCS) and subsequently assembled into the single AEMWE cell. A torque wrench was used to tighten the screws in the cell of materials to 3.5 N m.

2.8. Evaluation of ex-situ and in-situ alkaline stability

The ex-situ alkaline stability was tested as follows: the AEMs were submerged in NaOH (2 M and 5 M) solutions at 80 °C for a period of time to assess the changes in their ion conductivity and chemical composition. Meanwhile, the in-situ alkaline stability was performed at a constant current of 1 A cm⁻² at 80 °C in 1 M KOH, and the change of cell voltage and internal resistance were recorded to evaluate the durability.

3. Results and discussion

3.1. Synthesis and characterization of polymers

PFA-based copolymers were synthesized by a typical Friedel-Crafts

alkylation polymerization and quaternary ammonium functionalization. A certain proportion of diphenyl and *p*-triphenyl was introduced into the PFA to construct the combination of curved and straight segments, including PFBA-*x* and PFTA-*y*. The proportion of diphenyl and *p*-triphenyl was controlled by adjusting the feeding ratio with 9,9-dimethylfluorene. The obtained copolymer was basically consistent with the feed ratio, which was confirmed by the ^1H NMR spectra of the PFBr, PFBBR, and PFTBr (Fig. S1–S5).

In these ^1H NMR spectra, the chemical shift at 1.34 ppm is vested in the protons of side methyl on fluorenyl, and the two adjacent small peaks at 1.25 and 1.44 ppm are attributed to methylene on the long alkyl side chain [19]. The peaks at 7.25, 7.32, and 7.66 ppm belong to the chemical shifts of protons on fluorenyl groups [28]. Moreover, the percentage proportion of diphenyl and *p*-triphenyl chain segments on the whole polymer chain was calculated by the integral areas according to the equation of $(1 - 2(d + f + c - 2b)/6b) \times 100$. The results show the

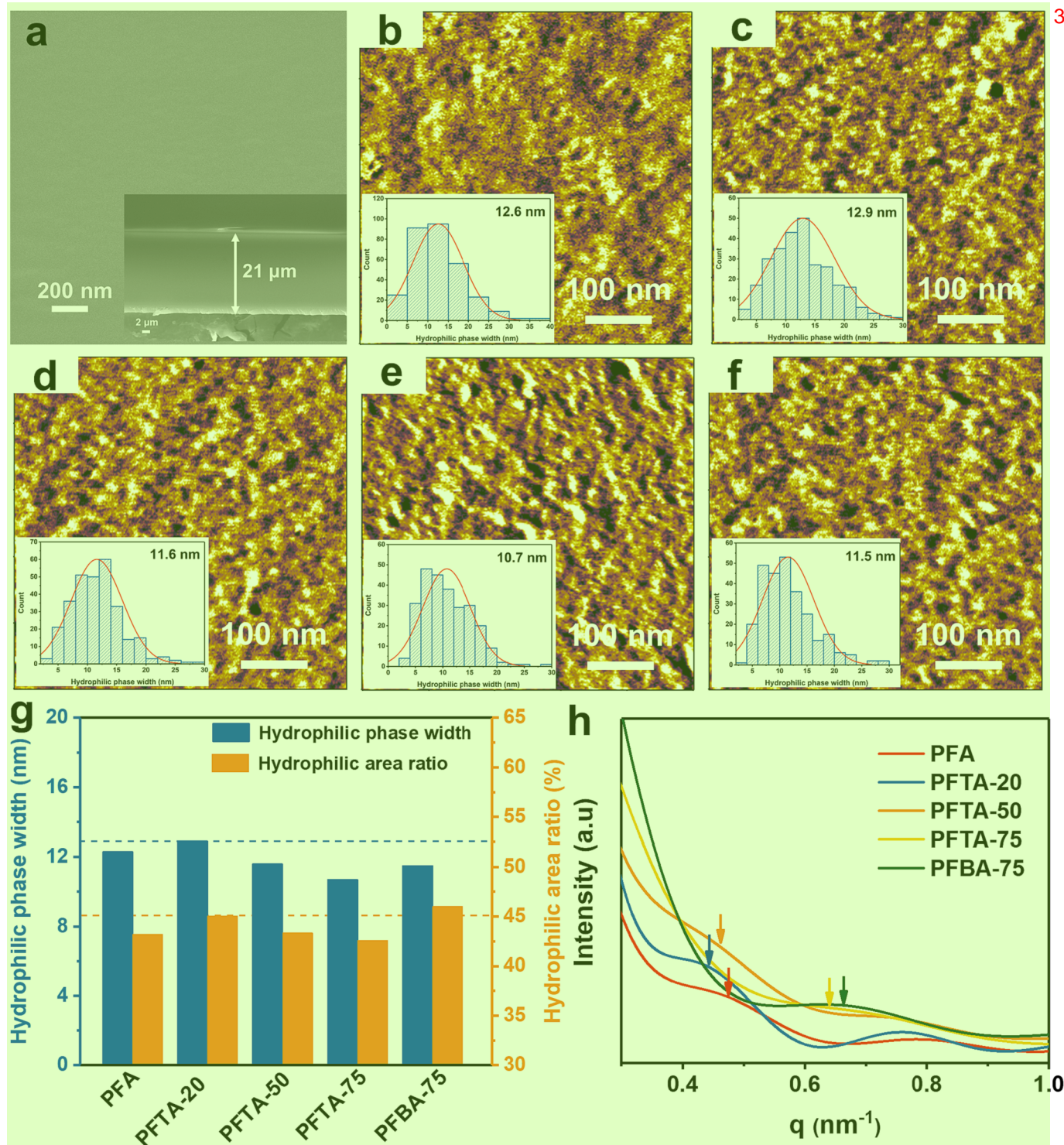


Fig. 2. Microstructural characterization of PFA-based AEMs. (a) SEM image of PFTA-20. AFM images of (b) PFA, (c) PFTA-20, (d) PFTA50, (e) PFTA75, and (f) PFBA-75. (g) The statistics of hydrophilic phase width and hydrophilic area ratio, and (h) SAXS spectra of PFA, PFBA-75, and PFTA-*y* (*y* = 20, 50, and 75) in Br^- form and dry state.

proportions are almost agreed with the designed value (Table S1). Fig. 1c show the ^1H NMR spectra of representative quaternized copolymers (others were displayed in Fig. S6-S7), in which the indicated chemical shifts are one-to-one correspondence with the chemical structures of copolymers.

3.2. Preparation and microstructure of AEMs

The AEMs, prepared by the solution casting method in this study, are flat and free of defects (Fig. 2a). It is known that well-structured and consecutive hydrophilic domains can facilitate ion conduction and reduce the hindrance of hydrophobic domain barriers, which are influenced by backbone structure, cations, linkage ways, and so on [29,30]. Fig. 2b-f show AFM phase images of as-prepared AEMs with different backbone structures, in which the light areas represent hydrophobic domains and the dark areas represent hydrophilic domains. The width and area ratio of the hydrophilic phase were summarized in Fig. 2g. The PFA membrane exhibits a well-defined microphase separation structure with 12.6 nm hydrophilic phase width and 43.2% hydrophilic area. The introduction of *p*-terphenyl in PFA further promotes the microphase separation, and thus the PFTA-20 membrane has a more broader hydrophilic phase (width of 12.9 nm, area ratio of 45.1%). But the hydrophilic phase becomes narrower and smaller as the *p*-terphenyl content further increases. However, the PFBA-75 AEM presents better microphase separation morphology than PFTA-75 AEM due to the higher IEC.

The microphase separation structure of AEMs was further confirmed

by SAXS profiles (Fig. 2h). It can be seen that the PFTA-20 AEM has the biggest ion cluster, and the domain spacing (d) is 14.2 nm after calculate according to Bragg's law ($d = 2\pi/q$). When the proportion of *p*-terphenyl and biphenyl was predominant, the resulted PFTA-75 and PFBA-75 membranes display smaller d . This dependence of d size on the structure is consistent with the AFM results, which further proves that the combination of curves and straight segments on the polymer backbone can effectively promote microphase separation. However, the PFBA-25 exhibited a smaller d , its hydrophilic phase width was higher than that of the PFTA-75 due to the much higher IEC (2.41), which generated more ionic clusters [31].

3.3. Dimensional stability, water uptake and OH^- conductivity

The swell behavior and hydration of PFA-based AEMs are greatly affected by the changes in the backbone structure. As shown in Fig. 3a, b, the PFA membrane presents a high SR of 45.8% and a high WU of 195.4%, which attributed to the rigid and curved backbone structure. However, the SR and WU significantly decreases with the content of biphenyl or *p*-terphenyl in the AEMs. The PFTA-75 presents the lowest SR and WU of 18.1% and 66.1%, which is much lower than that of PFBA-75 (SR = 41.4%, WU = 177.5%) and PFTA-20 (SR = 33.8%, WU = 128.7%). It demonstrates that the introduction of the *p*-terphenyl into PFA effectively relieved the swelling problem and maintained a suitable λ (Table S1).

The OH^- conductivity of the AEMs is displayed in Fig. 3c. Despite the PFTA- y and PFA AEMs having similar IEC (Table S1), the PFTA-20

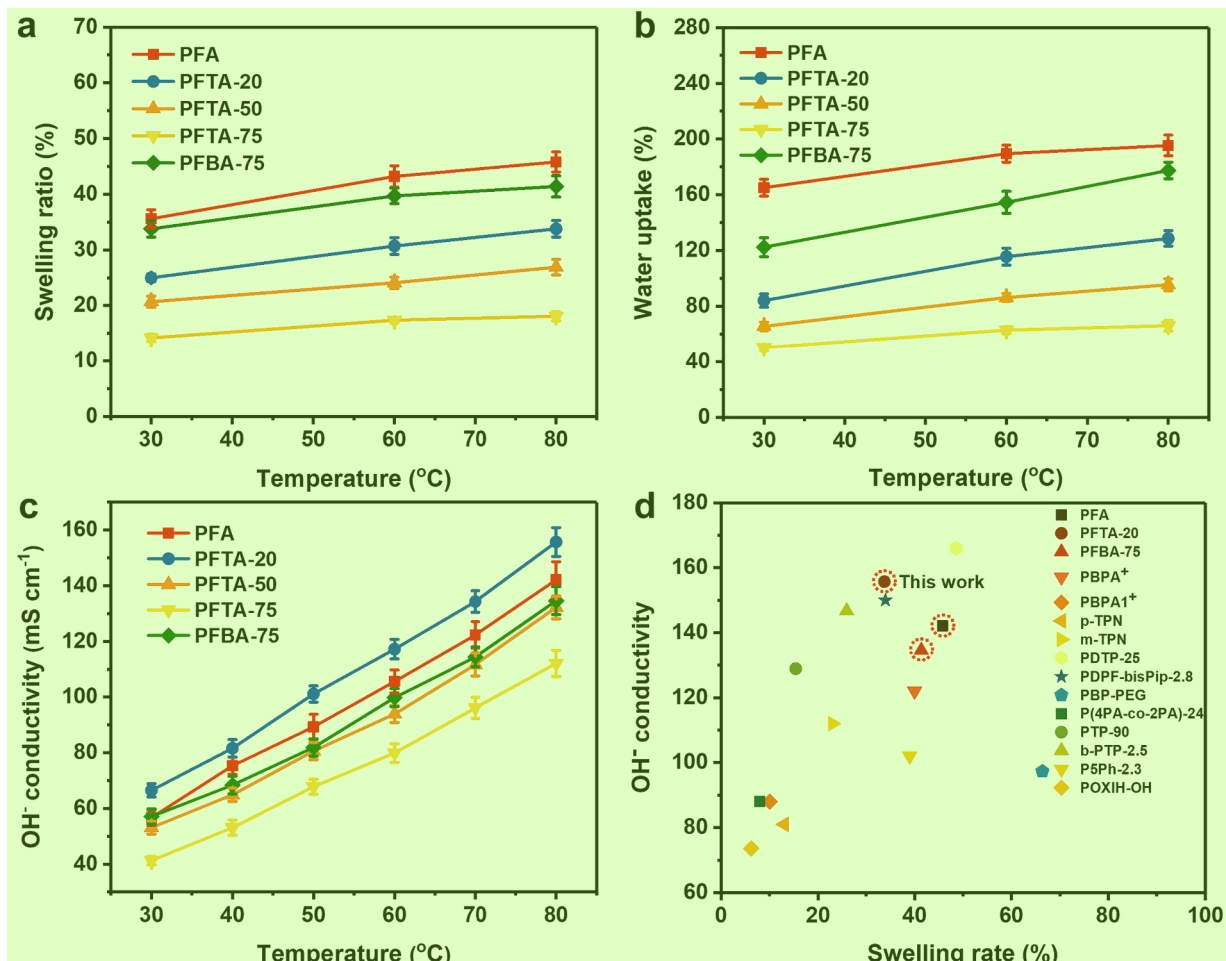


Fig. 3. Properties of PFA-based AEMs. (a, b, c) SR, WU and OH^- conductivity of PFA, PFBA-75, and PFTA- y ($y = 20, 50$, and 75), respectively. (d) The OH^- conductivity and swelling ratio comparison of PAF, PFBA-75, and PFTA-20 with state-of-the-art AEMs.

presents a higher OH^- conductivity of 155.7 mS cm^{-1} at 80°C than that of PFA (142.1 mS cm^{-1}) due to the well-defined microstructure [32]. As is well known, appropriate hydration can fill the hydrophilic domain (ionic domain) and enlarge ion transport channels in the AEM, and sufficient free water ensures the diffusion and electromigration of OH^- and forms a hydrogen-bond network of water molecules to facilitate OH^- transport [33]. But excess water in the high hydration will cause excess swelling and dilute the ion concentration, resulting in the decrease of the ion conductivity [34]. Among as-prepared AEMs, the PFBA-75 with the highest IEC possesses a lower OH^- conductivity of 134.6 mS cm^{-1} due to the poorer microphase separation structure (Table S1). Moreover, the activation energy (E_a) of prepared PFA-based AEMs is presented in Fig. S9, and PFTA-20 has the lowest E_a of 15.0 kJ mol^{-1} due to its well-defined microstructure. Compared with state-of-the-art AEMs (Fig. 3d), the PFTA-20 exhibits the advantages of high OH^- conductivity and low SR, which are highly competitive [21,22,27,35–41].

3.4. Mechanical, thermal and alkali stability

Rigid and curved fluorenyls in the polymer backbone also have a great influence on the mechanical properties of the membranes [28]. The mechanical property of as-prepared AEMs were measured at dry and wet state, respectively (Fig. 4a, b). And, the mechanical properties of all prepared AEMs are summarized in Table S2. The PFTA-75 presents the

best tensile stress (TS) of 44.7 MPa and elongation at break (EB) of 73.1% at dry state. By contrast, the mechanical properties in the wet state were noticeably improved because WU has a great influence on mechanical stability, but exorbitant water will cause a decrease in tensile strength [42]. The TS of PFA with high WU (195.4%) was dropped to 13.7 MPa , but the EB improved to 64.0% . However, the TS of PFTA-20 membrane was slight decreased to 22.3 MPa and achieved impressive EB of 71.9% with more appropriate WU (119.5%). The PFTA-y membranes present more predominant mechanical property than PFA and PFBA-75 attributing to the well-defined microstructure and suitable hydration.

In addition, the thermal stability of the AEMs was also evaluated (Fig. S10). Two mainly thermal degradation platforms were displayed, and all have a similar thermal decomposition process. The first stage of around 220°C to 370°C belonged to the degradation of long alkyl side chains, and the degradation of the polymer backbone occurred in the second stage of around 430°C to 580°C . Thus, the robust mechanical performance and good thermal stability of PFA-based AEMs completely satisfied the harsh working environment in AEMWE.

To evaluate chemical durability of PFA-based AEMs, the PFTA-20 was immersed in 2 M NaOH and 5 M NaOH at 80°C . The digital photos of PFTA-20 AEM before and after *ex-situ* alkali stability tests are shown in Fig. S12. And the changes in chemical structure and ion conductivity were recorded before and after the test. As displayed in Fig. 4c, the quaternary ammonium cationic group gradually degraded in 2 M

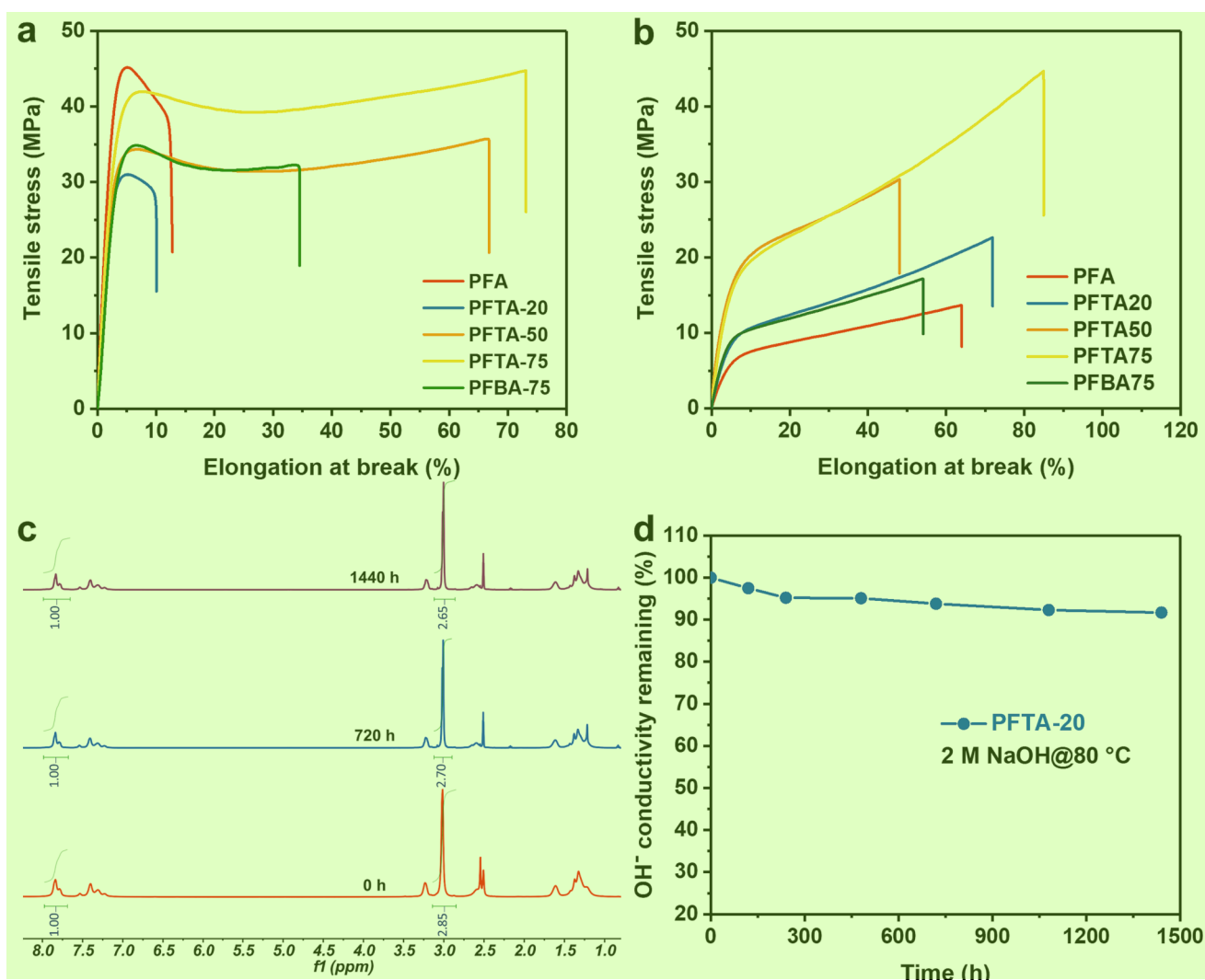


Fig. 4. (a, b) Mechanical properties of AEMs in Br^- form (dry) and in OH^- form (wet), respectively. (c) ¹H NMR spectra of PFTA-20 after an alkali stability test by immersion in 2 M NaOH (80°C) for a period of time. (d) The OH^- conductivity changes of PFTA-20 over the alkali stability test by immersion in 2 M NaOH (80°C).

NaOH, which degraded 7% by the calculation of the ^1H NMR integral area. And the OH^- conductivity decreased by 8.3% due to the degradation of the cationic group (Fig. 4d). In order to further investigate the change in chemical structure, the harsher condition of 5 M NaOH was used. Some new peaks emerged after immersion for 1440 h due to the degradation of cationic groups by nucleophilic substitution and Hofmann elimination, which was confirmed by the ^1H NMR spectrum (Fig. S8) [43]. The cationic groups lost 16.5% in the PFTA-20 AEM. In summary, the PFTA-20 AEM, with its considerable and excellent performance, is suitable for AEMWE applications.

3.5. Water electrolysis performance 2

The PTFA-20 AEM, with its highest ion conductivity and durable properties, was used in the AEMWE to get better performance. Ionomer is a critical influence factor on the AEMWE performance and plays the dual roles of binding catalyst and ion conduction. Thus, different ionomer species, ionomer contents, MEA preparation methods, and cell operation temperatures were investigated on the PTFA-20-based MEA to explore the effect of ionomer on the performance of AEMWE.

The polarization curves of different ionomer contents in the anode and cathode were investigated with the PFTA-20 as the ionomer. When the cathode ionomer content was increased from 20 wt% to 25 wt%, the highest current density of 4.9 A cm^{-2} at 2 V was achieved (Fig. 5a). The current decreased to 3.3 A cm^{-2} at 2 V as the cathode ionomer content continually increases to 35 wt%. The Nyquist plots of the relatively

AEMWE system are shown in Fig. 5b, which resulted from EIS analysis. A suitable cathode ionomer content of 25 wt% can reduce the ohmic resistance (R_{Ohm}) and charge transfer resistance (R_{CT}) to $0.0139 \Omega \text{ cm}^{-2}$ and $0.0217 \Omega \text{ cm}^{-2}$, respectively. However, excessive ionomer content of 35 wt% reduced the effective catalyst active sites and hindered the mass transfer, resulting in a higher R_{Ohm} of $0.0188 \Omega \text{ cm}^{-2}$ and R_{CT} of $0.0225 \Omega \text{ cm}^{-2}$. After the anode ionomer content increased to 10 wt%, the current density of cell decreased to 3.8 A cm^{-2} at 2 V with R_{Ohm} of $0.0159 \Omega \text{ cm}^{-2}$ and R_{CT} of $0.0219 \Omega \text{ cm}^{-2}$ (Fig. 5c, d). Importantly, the PFTA-20 based AEMWE with half catalyst load (1.0 mg cm^{-2} of IrO_2 and 0.5 mg cm^{-2} of Pt/C) still maintained a high current density of 4.2 A cm^{-2} at 2 V. When changing the electrolyte from 1 M KOH to 0.1 M KOH and pure water, the R_{Ohm} and R_{CT} significantly increased (Fig. S14b). The current densities significantly decreased to 3.3 and 0.9 A cm^{-2} at 2 V in 0.1 M KOH and pure water due to the high R_{Ohm} and R_{CT} , respectively (Fig. S14a). In addition, the PFTA-20-based AEMWE presented low electrolysis stability in 0.1 M KOH and pure water (Fig. S14c, d).

Except for the influence of ionomer content, the ionomer type is also important to the construction of the catalyst layer to obtain excellent AEMWE performance [4,8,10]. The lower current density of 4.6 A cm^{-2} (PFA as an ionomer) and 4.0 A cm^{-2} (PFBA-75 as an ionomer) at 2 V was presented (Fig. 6a, b), which was consistent with the variation trend of OH^- conductivity. The CCM and catalyst-coated substrate (CCS), two traditional preparation methods of MEA, have extensive application in AEMWE [44,45]. The AEMWE assembled by the CCS method presented a lower current density of 3.9 A cm^{-2} at 2.0 V with a higher internal

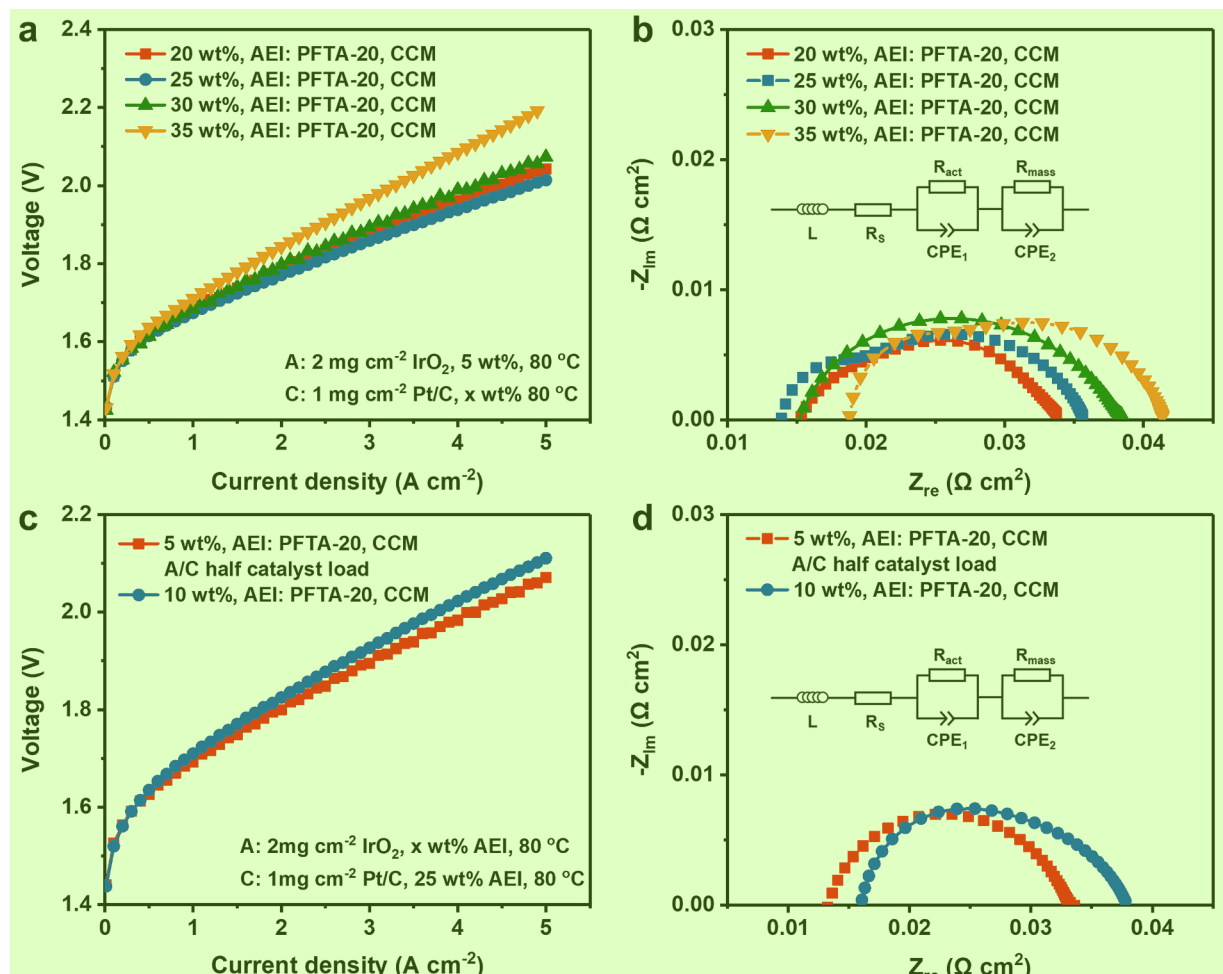


Fig. 5. Effect of ionomer content and catalyst loading on the performance of PFTA-20-based AEMWE. (a, b) Effect of cathode ionomer content on polarization curves and Nyquist plots. (c, d) Polarization curves and Nyquist plots of AEMWE with 10 wt% anode ionomer content and 5 wt% anode ionomer content (A/C half catalyst load). The MEAs were manufactured by the CCM method, and performed in 1 M KOH at 80 °C.

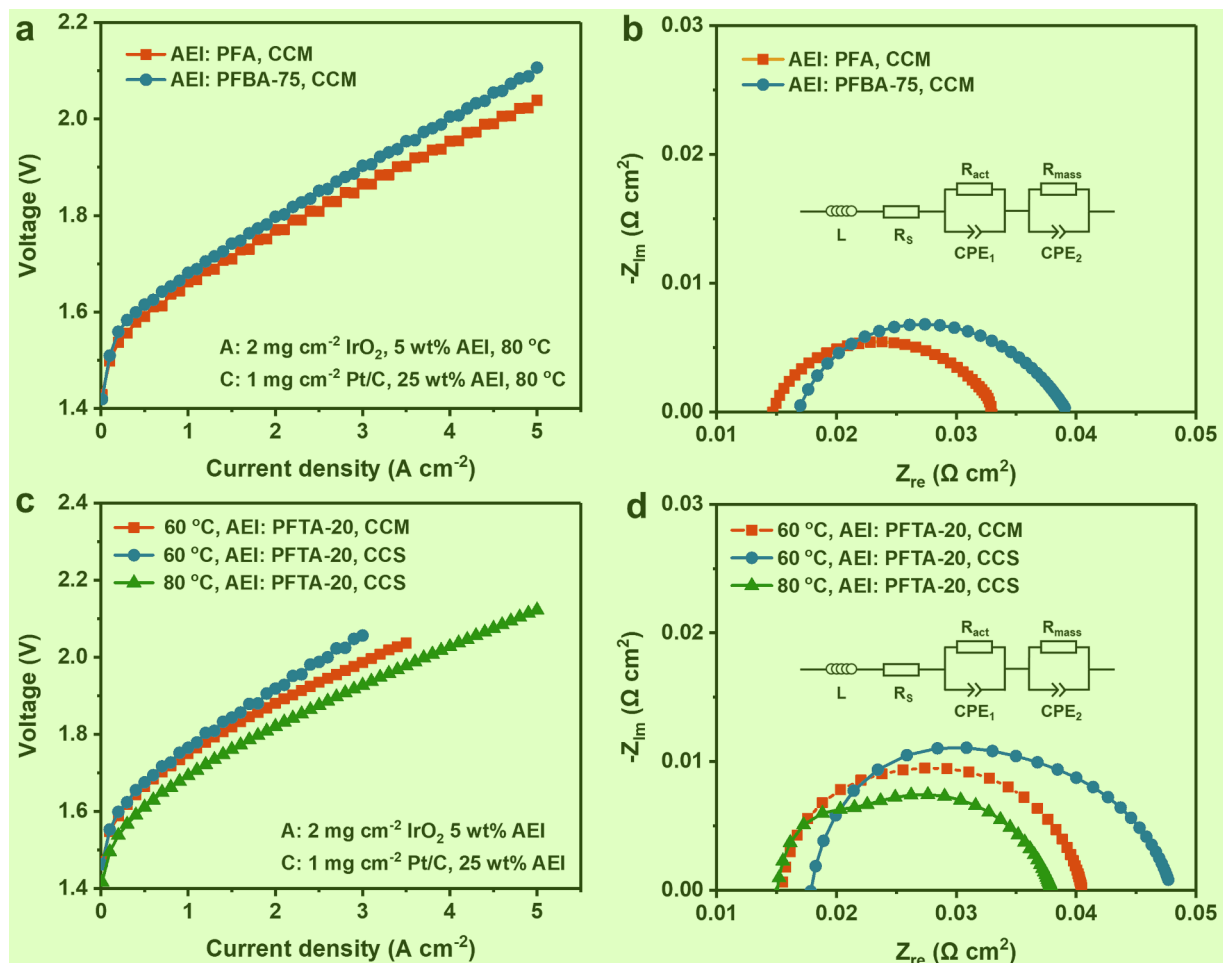


Fig. 6. The effect of different ionomers and the CCS MEA preparation method on the performance of PFTA-20-based AEMWE. (a) Polarization curves and (b) Nyquist plots of AEMWE with different ionomers at 80 °C. (c) Polarization curves and (d) Nyquist plots of AEMWE with the CCM and CCS methods prepared MEA.

resistance (Fig. 6c, d). Its AEMWE performance dropped significantly as the operating temperature was decreased to 60 °C, which attributed to the decreasing ionic conductivity and catalytic activity with the temperature (Fig. 6c) [46]. This result was confirmed by the increased R_{Ohm} ($0.0179 \Omega \text{ cm}^{-2}$) and R_{CT} ($0.0298 \Omega \text{ cm}^{-2}$) that are showed in Fig. 6d.

The long-term durability of PTFA-20-based AEMWE was tested in 1 M KOH at 80 °C with a constant current density of 1 A cm^{-2} , in which the MEA was prepared by the CCM method and the PFTA-20 as the ionomer. Fig. 7a shows the change of cell voltage with time in the 2200 h test. The cell voltage was stable at 1.84 V after 2200 h with a slow voltage rise rate of $77 \mu\text{V h}^{-1}$. In the first 400 h, the cell voltage experienced a rapid rise term from 1.67 V to 1.80 V. Presumably, catalyst activity loss, ionomer oxidation, or catalyst shedding caused this performance decay [8,14,52]. Furthermore, the R_{Ohm} and R_{CT} increased to $0.0278 \Omega \text{ cm}^{-2}$ and $0.0282 \Omega \text{ cm}^{-2}$ after 2200 h test (Fig. 7b). The AEM was peeled from the MEA after test, and characterized by ^1H NMR (Fig. S11). PFTA-20 exhibits good *in-situ* stability with QA groups only degraded by 13.7%, which attributes to a well-defined microstructure and an ether-free backbone structure [18,20,21]. The AEMWE performance of commercial AEM Sustainion® 37–50 Grade RT (Dioxide Materials, 50 μm) with the same test condition was conducted to compare. The lower current density of 2.6 A cm^{-2} at 2 V and high R_{Ohm} of $0.0224 \Omega \text{ cm}^{-2}$ are presented (Fig. S16a, b). And the voltage rises rapidly from 1.74 V to 2.02 V after operating for 300 h (Fig. S16c). Furthermore, the *in-situ* long-term durability AEMWE test of PFTA-20 AEM with the CCS MEA preparation method is displayed in Fig. S15, which operated for 250 h with a voltage decay rate of $240 \mu\text{V h}^{-1}$ (the voltage rises from

1.69 V to 1.75 V). High current density and 2200 h long-term stable water electrolysis operation of PFTA-20 outperformed most reported AEMWE performance (Fig. 7c) [4,8,10,12,44,45,47–51].

4. Conclusions

In this study, we presented a series of PFA-based AEMs combined with different contents of *p*-terphenyl or biphenyl. The combination of fluorenyl and *p*-terphenyl in PFTA has been demonstrated to help construct a well-defined microphase separation structure that facilitates ionic conduction. The PFTA-20 AEM presents a high OH^- conductivity of 155.7 mS cm^{-2} with a low SR of 33.8% and a high WU of 128.7% by introducing a suitable content of *p*-terphenyl into PFA. Meanwhile, robust mechanical properties in the wet state (TS = 22.3 MPa, EB = 71.9%) and durable alkaline stability (after soaking in 2 M NaOH at 80 °C for 1440 h, cationic groups remained at 93%) of PFTA-20 can well meet the harsh high temperature alkaline working environment of AEMWE. The PTFA-20-based AEMWE achieved a high current density of 4.9 A cm^{-2} at 2 V and stable operation for 2200 h with a slow voltage rising rate of $77 \mu\text{V h}^{-1}$ in 1 A cm^{-2} constant current model (1 M KOH, 80 °C). In summary, biphenyl and *p*-triphenyl were introduced into PFA to construct PFBA and PFTA polymer structures, which shed light on the relationship between structure and performance in AEM. The developed AEMs should have a wide application in the AEMWE.

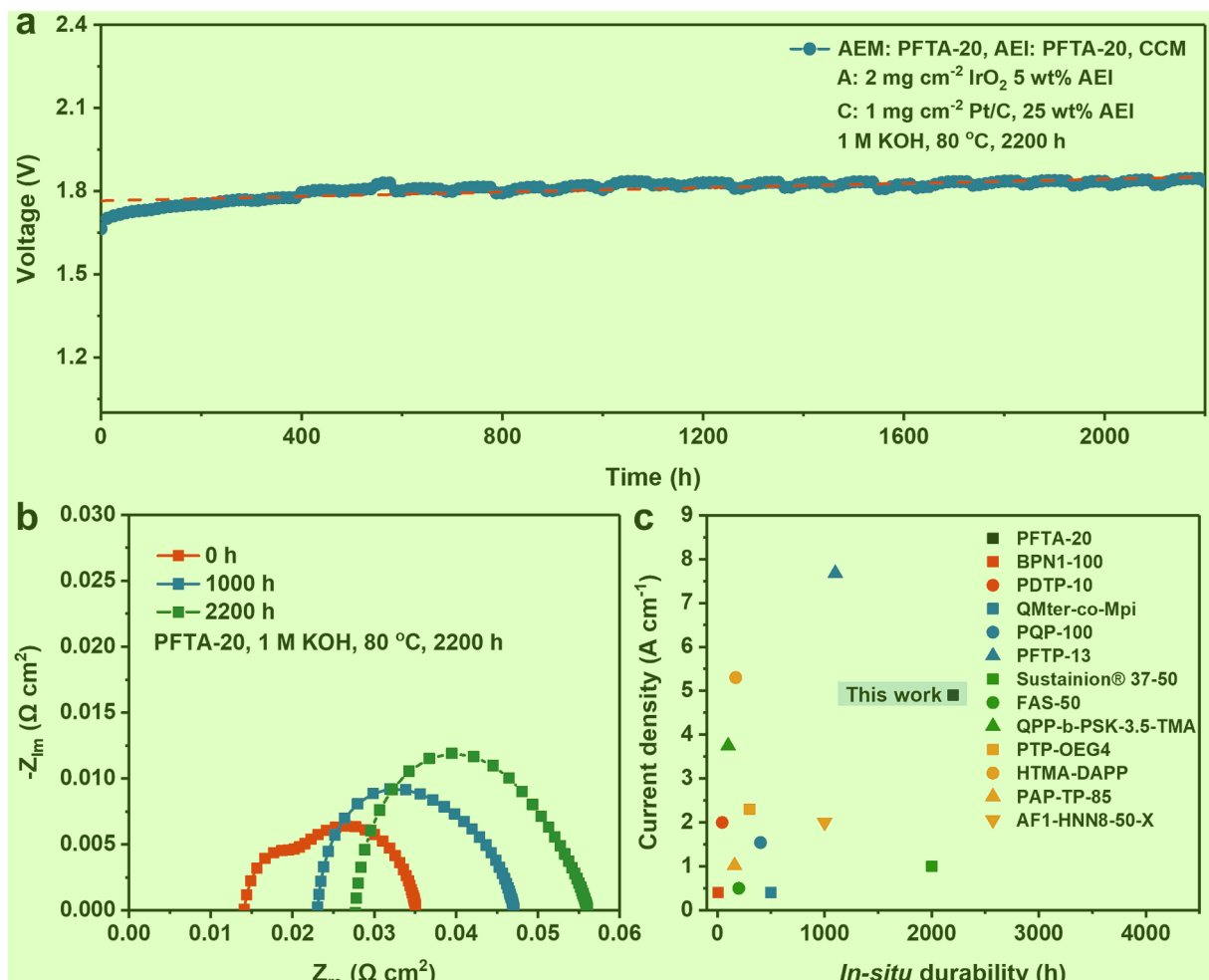


Fig. 7. In-situ long-term durability AEMWE test of PFTA-20 AEM in 1 M KOH at 80 °C with a constant current density of 1 A cm⁻². (a) Voltage changes with in-situ test time. (b) Nyquist plots of PFTA-20-based AEMWE in different periods of in-situ test. (c) The achieved current density and in-situ durability test duration comparison of PFTA-20-based AEMWE with state-of-the-art AEMWEs. The current density of PFTA-20 AEM was recorded at 2.0 V, BPN1-100 and PDTP-10 were recorded at 2.1 V [47,48], QMter-co-Mpi, PQP-100, and PFTP-13 were recorded at 2.0 V [4,49,50], Sustainion® 37-50, FSA-50, and QPP-b-PSK-3.5-TMA were recorded at 1.9 V [12,44], PTP-OEG4, HTMA-DAPP, PAP-TP-85, and AF1-HNN8-50-X were recorded at 1.8 V [8,10,45,51]. Furthermore, the test details of the compared AEMWEs were displayed in Table S3.

CRediT authorship contribution statement 3

Yichang Ma: Data curation, Formal analysis, Investigation, Methodology, Visualization, Writing – original draft, Writing – review & editing. **Lingjing Li:** Formal analysis, Investigation, Data curation. **Xueqing You:** Formal analysis, Investigation. **Huiting Lin:** Formal analysis. **Guiqin Yi:** Formal analysis. **Xiangyu Su:** Formal analysis. **Aimei Zhu:** Formal analysis. **Qinglin Liu:** Formal analysis. **Qiugen Zhang:** Conceptualization, Data curation, Supervision, Project administration, Writing – review & editing, Writing – original draft.

Acknowledgments 5

This work is supported by the National Nature Science Foundation of China (No. 22178292), Science and Technology Planning Project of Fujian Province of China (No. 2020H0003).

Appendix A. Supplementary data 7

Supplementary data to this article can be found online at <https://doi.org/10.1016/j.cej.2023.148225>.

References 13

- [1] Y. Yang, P. Li, X. Zheng, W. Sun, S.X. Dou, T. Ma, H. Pan, Anion-exchange membrane water electrolyzers and fuel cells, Chem. Soc. Rev. 51 (23) (2022) 9620–9693, <https://doi.org/10.1039/d2cs00038e>.
- [2] A. Hodges, A.L. Hoang, G. Tsekouras, K. Wagner, C.Y. Lee, G.F. Swiegers, G. Wallace, A high-performance capillary-fed electrolysis cell promises more cost-competitive renewable hydrogen, Nat. Commun. 13 (1) (2022) 1304, <https://doi.org/10.1038/s41467-022-28953-x>.
- [3] R. Abbasi, B.P. Setzler, S. Lin, J. Wang, Y. Zhao, H. Xu, B. Pivovar, B. Tian, X. Chen, G. Wu, Y. Yan, A roadmap to low-cost hydrogen with hydroxide exchange membrane electrolyzers, Adv. Mater. 31 (31) (2019) e1805876.
- [4] N. Chen, S.Y. Paek, J.Y. Lee, J.H. Park, S.Y. Lee, Y.M. Lee, High-performance anion exchange membrane water electrolyzers with a current density of 7.68 A cm⁻² and

Declaration of competing interest 9

The authors declare that they have no known competing financial interests or personal relationships that could have appeared to influence the work reported in this paper.

Data availability 11

Data will be made available on request. 12

- a durability of 1000 hours, *Energy Environ. Sci.* 14 (12) (2021) 6338–6348. <https://doi.org/10.1039/d1ee02642a>.
- [5] L. Wan, Z. Xu, Q. Xu, M. Pang, D. Lin, J. Liu, B. Wang, Key components and design strategy of the membrane electrode assembly for alkaline water electrolysis, *Energy Environ. Sci.* 16 (4) (2023) 1384–1430, <https://doi.org/10.1039/d3ee00142c>.
 - [6] F. Razmjooei, T. Morawietz, E. Taghizadeh, E. Hadjixenophontos, L. Mues, M. Gerle, B.D. Wood, C. Harms, A.S. Gago, S.A. Ansar, K.A. Friedrich, Increasing the performance of an anion-exchange membrane electrolyzer operating in pure water with a nickel-based microporous layer, *Joule* 5 (7) (2021) 1776–1799, <https://doi.org/10.1016/j.joule.2021.05.006>.
 - [7] A.W. Tricker, J.K. Lee, J.R. Shin, N. Danilovic, A.Z. Weber, X. Peng, Design and operating principles for high-performing anion exchange membrane water electrolyzers, *J. Power Sources* 567 (2023), 232967, <https://doi.org/10.1016/j.jpowsour.2023.232967>.
 - [8] D. Li, E.J. Park, W. Zhu, Q. Shi, Y. Zhou, H. Tian, Y. Lin, A. Serov, B. Zulevi, E. D. Baca, C. Fujimoto, H.T. Chung, Y.S. Kim, Highly quaternized polystyrene ionomers for high performance anion exchange membrane water electrolyzers, *Nat. Energy* 5 (5) (2020) 378–385, <https://doi.org/10.1038/s41560-020-0577-x>.
 - [9] L. Wan, J. Liu, Z. Xu, Q. Xu, M. Pang, P. Wang, B. Wang, Construction of integrated electrodes with transport highways for pure-water-fed anion exchange membrane water electrolysis, *Small* 18 (21) (2022), 2200380, <https://doi.org/10.1002/smll.202200380>.
 - [10] P. Fortin, T. Khoza, X. Cao, S.Y. Martinsen, A. Oyarce Barnett, S. Holdcroft, High-performance alkaline water electrolysis using Aemion™ anion exchange membranes, *J. Power Sources* 451 (2020), 227814, <https://doi.org/10.1016/j.jpowsour.2020.227814>.
 - [11] D. Henkensmeier, M. Najibah, C. Harms, J. Žitka, J. Hnátek, K. Bouzek, Overview: state-of-the art commercial membranes for anion exchange membrane water electrolysis, *J. Electrochem. Energy Convers. Storage* 18 (2) (2021), 024001, <https://doi.org/10.1115/1.4047963>.
 - [12] Z. Liu, S.D. Sajjad, Y. Gao, H. Yang, J.J. Kaczur, R.I. Masel, The effect of membrane on an alkaline water electrolyzer, *Int. J. Hydrogen Energy* 42 (50) (2017) 29661–29665, <https://doi.org/10.1016/j.ijhydene.2017.10.050>.
 - [13] G.A. Lindquist, S.Z. Oener, R. Krivina, A.R. Motz, A. Keane, C. Capuano, K.E. Ayers, S.W. Boettcher, Performance and durability of pure-water-fed anion exchange membrane electrolyzers using baseline materials and operation, *ACS Appl. Mater. Interfaces* 13 (44) (2021) 51917–51924, <https://doi.org/10.1021/acsmami.1c06053>.
 - [14] D. Li, A.R. Motz, C. Bae, C. Fujimoto, G. Yang, F.-Y. Zhang, K.E. Ayers, Y.S. Kim, Durability of anion exchange membrane water electrolyzers, *Energy Environ. Sci.* 14 (6) (2021) 3393–3419, <https://doi.org/10.1039/d0ee04086j>.
 - [15] Z. Xu, V. Wilke, J.J. Chmielarz, M. Tobias, V. Atanasov, A.S. Gago, K.A. Friedrich, Novel piperidinium-functionalized crosslinked anion exchange membrane with flexible spacers for water electrolysis, *J. Membr. Sci.* 670 (2023), 121302, <https://doi.org/10.1016/j.memsci.2022.121302>.
 - [16] H. Chen, R. Tao, K.T. Bang, M. Shao, Y. Kim, Anion exchange membranes for fuel cells: state-of-the-art and perspectives, *Adv. Energy Mater.* 12 (28) (2022) 2200934, <https://doi.org/10.1002/aenm.202200934>.
 - [17] J.S. Olsson, T.H. Pham, P. Jannasch, Poly(arylene piperidinium) hydroxide ion exchange membranes: synthesis, alkaline stability, and conductivity, *Adv. Funct. Mater.* 28 (2) (2018) 1702758, <https://doi.org/10.1002/adfm.201702758>.
 - [18] M.S. Cha, J.E. Park, S. Kim, S.-H. Han, S.-H. Shin, S.H. Yang, T.-H. Kim, D.M. Yu, S. So, Y.T. Hong, S.J. Yoon, S.-G. Oh, S.Y. Kang, O.-H. Kim, H.S. Park, B. Bae, Y.-E. Sung, Y.-H. Cho, J.Y. Lee, Poly(carbazole)-based anion-conducting materials with high performance and durability for energy conversion devices, *Energy Environ. Sci.* 13 (10) (2020) 3633–3645, <https://doi.org/10.1039/d0ee01842b>.
 - [19] S. Maurya, S. Noh, I. Matanovic, E.J. Park, C. Narvaez Villarrubia, U. Martinez, J. Han, C. Bae, Y.S. Kim, Rational design of polyaromatic ionomers for alkaline membrane fuel cells with > 1 W cm⁻² power density, *Energy Environ. Sci.* 11(11) (2018) 3283–3291, <https://doi.org/10.1039/c8ee02192a>.
 - [20] S. Zhang, X. Zhu, C. Jin, Development of a high-performance anion exchange membrane using poly(isatis biphenylene) with flexible heterocyclic quaternary ammonium cations for alkaline fuel cells, *J. Mater. Chem. A* 7 (12) (2019) 6883–6893, <https://doi.org/10.1039/c8ta11291f>.
 - [21] W.H. Lee, Y.S. Kim, C. Bae, Robust hydroxide ion conducting poly(biphenyl alkylene)s for alkaline fuel cell membranes, *ACS Macro Lett.* 4 (8) (2015) 814–818, <https://doi.org/10.1021/acsmacrolett.5b00375>.
 - [22] W.H. Lee, E.J. Park, J. Han, D.W. Shin, Y.S. Kim, C. Bae, Poly(terphenylene) anion exchange membranes: the effect of backbone structure on morphology and membrane property, *ACS Macro Lett.* 6 (5) (2017) 566–570, <https://doi.org/10.1021/acsmacrolett.7b00148>.
 - [23] I. Matanovic, S. Maurya, E.J. Park, J.Y. Jeon, C. Bae, Y.S. Kim, Adsorption of polyaromatic backbone impacts the performance of anion exchange membrane fuel cells, *Chem. Mater.* 31 (11) (2019) 4195–4204, <https://doi.org/10.1021/acs.chemmater.9b01092>.
 - [24] S. Maurya, J.H. Dumont, C.N. Villarrubia, I. Matanovic, D. Li, Y.S. Kim, S. Noh, J. Han, C. Bae, H.A. Miller, C.H. Fujimoto, D.R. Dekel, Surface adsorption affects the performance of alkaline anion-exchange membrane fuel cells, *ACS Catal.* 8 (10) (2018) 9429–9439, <https://doi.org/10.1021/acscatal.8b03227>.
 - [25] Y. Ma, C. Hu, G. Yi, Z. Jiang, X. Su, Q. Liu, J.Y. Lee, S.Y. Lee, Y.M. Lee, Q. Zhang, Durable multiblock poly(biphenyl alkylene) anion exchange membranes with microphase separation for hydrogen energy conversion, *Angew. Chem. Int. Ed.* 62 (41) (2023) e202311509.
 - [26] J. Wang, Y. Zhao, B.P. Setzler, S. Rojas-Carbonell, C. Ben Yehuda, A. Amel, M. Page, L. Wang, K. Hu, L. Shi, S. Gottesfeld, B. Xu, Y. Yan, Poly(aryl piperidinium)
- membranes and ionomers for hydroxide exchange membrane fuel cells, *Nat. Energy* 4(5) (2019) 392–398, <https://doi.org/10.1038/s41560-019-0372-8>.
- [27] N. Chen, C. Hu, H.H. Wang, S.P. Kim, H.M. Kim, W.H. Lee, J.Y. Bae, J.H. Park, Y.M. Lee, Poly(Alkyl-Terphenyl Piperidinium) Ionomers and Membranes with an Outstanding Alkaline-Membrane Fuel-Cell Performance of 2.58 W cm⁻², *Angew. Chem. Int. Ed.* 60(14) (2021) 7710–7718, <https://doi.org/10.1002/anie.202013395>.
 - [28] N. Chen, H.H. Wang, S.P. Kim, H.M. Kim, W.H. Lee, C. Hu, J.Y. Bae, E.S. Sim, Y. C. Chung, J.H. Jang, S.J. Yoo, Y. Zhuang, Y.M. Lee, Poly(fluorenyl aryl piperidinium) membranes and ionomers for anion exchange membrane fuel cells, *Nat. Commun.* 12 (1) (2021) 2367, <https://doi.org/10.1038/s41467-021-22612-3>.
 - [29] M. Hren, M. Božić, D. Fakin, K.S. Kleinschek, S. Gorgieva, Alkaline membrane fuel cells: anion exchange membranes and fuels, *Sustain. Energy Fuels* 5 (3) (2021) 604–637, <https://doi.org/10.1039/dose01373k>.
 - [30] B. Yang, Z. Cumman, Progress in constructing high-performance anion exchange membrane: molecular design, microphase controllability and in-device property, *Chem. Eng. J.* 457 (2023), 141094, <https://doi.org/10.1016/j.cej.2022.141094>.
 - [31] J. Chen, M. Guan, K. Li, S. Tang, Novel quaternary ammonium-functionalized covalent organic frameworks/poly(2,6-dimethyl-1,4-phenylene oxide) hybrid anion exchange membranes with enhanced ion conductivity and stability, *ACS Appl. Mater. Interfaces* 12 (13) (2020) 15138–15144, <https://doi.org/10.1021/acsm.9b22916>.
 - [32] X. Wu, N. Chen, C. Hu, H.A. Klok, Y.M. Lee, X. Hu, Fluorinated poly(aryl piperidinium) membranes for anion exchange membrane fuel cells, *Adv. Mater.* 35 (26) (2023) 2210432, <https://doi.org/10.1002/adma.202210432>.
 - [33] D.A. Salvatore, C.M. Gabardo, A. Reyes, C.P. O'Brien, S. Holdcroft, P. Pintauro, B. Bahar, M. Hickner, C. Bae, D. Sinton, E.H. Sargent, C.P. Berlinguet, Designing anion exchange membranes for CO₂ electrolyzers, *Nat. Energy* 6 (4) (2021) 339–348, <https://doi.org/10.1038/s41560-020-00761-x>.
 - [34] K.M. Lee, R. Wycisk, M. Litt, P.N. Pintauro, Alkaline fuel cell membranes from xylylene block ionenes, *J. Membr. Sci.* 383 (1–2) (2011) 254–261, <https://doi.org/10.1016/j.memsci.2011.08.062>.
 - [35] A. Allushi, T.H. Pham, P. Jannasch, Highly conductive hydroxide exchange membranes containing fluorene-units tethered with dual pairs of quaternary piperidinium cations, *J. Membr. Sci.* 632 (2021), 119376, <https://doi.org/10.1016/j.memsci.2021.119376>.
 - [36] L. Yang, Z. Wang, F. Wang, Z. Wang, H. Zhu, Poly(aryl piperidinium) anion exchange membranes with cationic extender sidechain for fuel cells, *J. Membr. Sci.* 653 (2022), 120448, <https://doi.org/10.1016/j.memsci.2022.120448>.
 - [37] T. Jiang, C. Wu, Y. Zhou, S. Cheng, S. Yang, H. Wei, Y. Ding, Y. Wu, Highly stable poly(p-quaterphephenylene alkylene)-based anion exchange membranes, *J. Membr. Sci.* 647 (2022), 120342, <https://doi.org/10.1016/j.memsci.2022.120342>.
 - [38] X. Wu, N. Chen, H.A. Klokk, Y.M. Lee, X. Hu, Branched poly(aryl piperidinium) membranes for anion-exchange membrane fuel cells, *Angew. Chem. Int. Ed.* 61 (7) (2022) e202114892.
 - [39] X. Hu, Y. Huang, L. Liu, Q. Ju, X. Zhou, X. Qiao, Z. Zheng, N. Li, Piperidinium functionalized aryl ether-free polyaromatics as anion exchange membrane for water electrolyzers: performance and durability, *J. Membr. Sci.* 621 (2021), 118964, <https://doi.org/10.1016/j.memsci.2020.118964>.
 - [40] T.H. Pham, J.S. Olsson, P. Jannasch, Poly(arylene alkylene)s with pendant N-spirocyclic quaternary ammonium cations for anion exchange membranes, *J. Mater. Chem. A* 6 (34) (2018) 16537–16547, <https://doi.org/10.1039/c8ta04699a>.
 - [41] R. Ren, S. Zhang, H.A. Miller, F. Vizza, J.R. Varcoe, Q. He, Facile preparation of novel cardo Poly(oxindolebiphenylene) with pendent quaternary ammonium by superacid-catalysed polyhydroxyalkylation reaction for anion exchange membranes, *J. Membr. Sci.* 591 (2019), 117320, <https://doi.org/10.1016/j.memsci.2019.117320>.
 - [42] W. Yuan, L. Zeng, Y. Li, J. Wang, X. Wang, Q. Liao, L. Li, Z. Wei, Ultrathin and super strong UHMWPE supported composite anion exchange membranes with outstanding fuel cells performance, *Small* 18 (10) (2022) e2105499.
 - [43] S. Xu, W. Wei, X. Su, R. He, Crown-ether block copolymer based poly(isatin terphenyl) anion exchange membranes for electrochemical energy conversion devices, *Chem. Eng. J.* 455 (2023), 140776, <https://doi.org/10.1016/j.cej.2022.140776>.
 - [44] M.S. Cha, J.E. Park, S. Kim, S.-H. Shin, S.H. Yang, S.J. Lee, T.-H. Kim, D.M. Yu, S. So, K.M. Oh, Y.-E. Sung, Y.-H. Cho, J.Y. Lee, Oligomeric chain extender-derived anion conducting membrane materials with poly(p-phenylene)-based architecture for fuel cells and water electrolyzers, *J. Mater. Chem. A* 10 (17) (2022) 9693–9706, <https://doi.org/10.1039/c1ta10868a>.
 - [45] L. Liu, L. Bai, Z. Liu, S. Miao, J. Pan, L. Shen, Y. Shi, N. Li, Side-chain structural engineering on poly(terphenyl piperidinium) anion exchange membrane for water electrolyzers, *J. Membr. Sci.* 665 (2023), 121135, <https://doi.org/10.1016/j.memsci.2022.121135>.
 - [46] C. Chen, Y.L. Tse, G.E. Lindberg, C. Knight, G.A. Voth, Hydroxide solvation and transport in anion exchange membranes, *J. Am. Chem. Soc.* 138 (3) (2016) 991–1000, <https://doi.org/10.1021/jacs.5b11951>.
 - [47] E.J. Park, C.B. Capuano, K.E. Ayers, C. Bae, Chemically durable polymer electrolytes for solid-state alkaline water electrolysis, *J. Power Sources* 375 (2018) 367–372, <https://doi.org/10.1016/j.jpowsour.2017.07.090>.
 - [48] X. Wang, X. Qiao, S. Liu, L. Liu, N. Li, Poly(terphenyl piperidinium) containing hydrophilic crown ether units in main chains as anion exchange membranes for alkaline fuel cells and water electrolyzers, *J. Membr. Sci.* 653 (2022), 120558, <https://doi.org/10.1016/j.memsci.2022.120558>.
 - [49] M. Liu, X. Hu, B. Hu, L. Liu, N. Li, Soluble poly(aryl piperidinium) with extended aromatic segments as anion exchange membranes for alkaline fuel cells and water

- electrolysis, *J. Membr. Sci.* 642 (2022), 119966, <https://doi.org/10.1016/j.memsci.2021.119966>. 1
- [50] X. Yan, X. Yang, X. Su, L. Gao, J. Zhao, L. Hu, M. Di, T. Li, X. Ruan, G. He, Twisted ether-free polymer based alkaline membrane for high-performance water electrolysis, *J. Power Sources* 480 (2020), 228805, <https://doi.org/10.1016/j.jpowsour.2020.228805>.
- [51] J. Xiao, A.M. Oliveira, L. Wang, Y. Zhao, T. Wang, J. Wang, B.P. Setzler, Y. Yan, Water-fed hydroxide exchange membrane electrolyzer enabled by a fluoride- incorporated nickel-iron oxyhydroxide oxygen evolution electrode, *ACS Catal.* 11 (1) (2020) 264–270, <https://doi.org/10.1021/acscatal.0c04200>. 2
- [52] J. Hyun, S. Hwan Yang, D. Wook Lee, E. Oh, H. Bae, M. Suc Cha, G. Doo, J. Yong Lee, H.-T. Kim, Impact of the binding ability of anion exchange ionomer on the initial performance degradation of anion exchange membrane water electrolyzers, *Chem. Eng. J.* 469 (2023), 143919, <https://doi.org/10.1016/j.cej.2023.143919>.